IMPACT OF THE ASSOCIATED CATION ON CHLORIDE BINDING OF PORTLAND CEMENT PASTE

K. De Weerdt (1), A. Colombo (1,2), L. Coppola (2), H. Justnes (3), M.R. Geiker (1)

(1) Department of Structural Engineering, Norwegian University of science and Technology, Norway

(2) Department of Engineering, University of Bergamo, Italy

(3) SINTEF Building and Infrastructure, Trondheim, Norway

ABSTRACT

Well hydrated cement paste was exposed to $MgCl_2$, $CaCl_2$ and NaCl solutions at 20°C. The chloride binding isotherms for free chloride concentrations ranging up to 1.5 mol/l were determined experimentally. More chlorides were found to be bound when the associated cation was Mg^{2+} or Ca^{2+} compared to Na^{+}. The chloride binding capacity of the paste appeared to be related to the pH of the exposure solution. In order to explain the cation dependency of the chloride binding a selection of samples was investigated in detail using experimental techniques such as TG, XRD and SEM-EDS to identify the phases binding the chlorides. The experimentally obtained data were compared with the calculations of a thermodynamic model, GEMS. It is concluded that the measured change in chloride binding depending on the cation was mainly governed by the pH of the exposure solution and thereby the binding capacity of the C-S-H.

KEYWORDS

chloride binding, cement, cation, SEM-EDS, pH

1 INTRODUCTION

Reinforced concrete structures exposed to chlorides from e.g. de-icing salts or sea water have a limited service life due to pitting corrosion of the steel reinforcement. The chlorides propagate through the concrete cover and disrupt locally the protective layer at the surface of the steel reinforcement causing corrosion of the steel when reaching a critical level.

When a concrete structure is assessed for chloride intrusion generally the total chloride content is determined at varying depths from the exposed surface. Part of the chlorides is bound in reaction products such as Friedel's salts or adsorbed on the calcium silicate hydrates (C-S-H) and part of it is retained in the pore solution. It is the free chloride content, the chlorides retained in the pore solution, which are considered to be ones able to move and which can cause pitting corrosion of the steel reinforcement. Hence, binding of chlorides in the hydration phases can lower the chloride concentration in the pore solution and reduce the rate of chloride ingress as well as lower the free chloride concentration near the steel.

An understanding of the chloride binding mechanisms is required in order to assess the chloride ingress and the risk of corrosion thereby potentially improving predictions of the service life of reinforced concrete structures.

2 BACKGROUND

When studying chloride binding of concrete, cement paste or mortar, chlorides can be introduced internally e.g. by addition to the mixing water or they can be introduced externally by exposing hydrated samples to chloride containing solutions. Internally introduced chlorides affect the hydration of the cement and the microstructure of the hardened cement paste [1].

In this study the focus will be on the exposure to external chlorides meaning exposing hardened cement paste to solutions containing chlorides as this is more representative for chloride ingress in concrete.

Most research on chloride binding of concrete has been done on binding from NaCl [2-7]. This is one of the main de-icing agents used on roads and bridges and the major component of sea water and is thus relevant for marine exposed concrete structures. However $CaCl_2$ and $MgCl_2$ are also used as de-icing agents as they suppress the freezing temperature even more than NaCl, and in addition they are applied as road dust-binders in for example tunnels [8]. In addition, Mg and Ca are together with S the major ions present in sea water after Na and Cl. Hence, cations other than Na such as Ca and Mg are of interest when studying chloride binding in concrete.

It has been shown that the cation associated with chloride plays an important role regarding chloride binding [9-13]. Exposure of concrete to $CaCl_2$ has been found to result in more bound chlorides compared to NaCl. $MgCl_2$ behaves similarly as $CaCl_2$ [10, 13] as well as HCl [10].

The increased chloride binding for $CaCl_2$ compared with NaCl has been observed to coincide with a decrease in pH in the pore solution [9, 12, 13]. However the hypotheses for the link between increased chloride binding and decrease in pH vary. Tritthart [9] proposed that the observed decrease in the OH^- concentration of the pore solution for $CaCl_2$ and $MgCl_2$ exposure solutions can be attributed to the precipitation of $Ca(OH)_2$ and $Mg(OH)_2$ equivalently with the quantity of the chloride salt added. The inverse relation between the OH^- concentration of the pore water and chloride binding of the cement paste indicates that chlorides are bound through competing adsorption between Cl^- and OH^-, according to Tritthart [9]. Wowra and Setzer [12] proposed that the decrease in the pH is caused by sorption of

Ca^{2+} ions on the surface of the C-S-H, rendering the surface positively charged thereby leading to the adsorption of counter ions such as OH^- and Cl^-. Arya et al. [10] and Zhu et al. [13] mention the effect of pH on the solubility of the AFm and AFt phases. Their explanations for the relationship between pH and chloride binding are incomplete and not confirmed experimentally.

The present study is designed to bring the understanding of the impact of the associated cation a step further compared with the above mentioned studies by not only determining the overall chloride binding and in some cases the pH of the exposure solution, but also explaining the cause of these changes. This was done by analysing in a controlled set-up the changes in the elemental composition of the exposure solution and the phase assemblage of a well hydrated cement paste exposed to $MgCl_2$, $CaCl_2$ and NaCl solutions. In addition, the experimental results are compared with the phase changes and changes in the pore solution predicted by a thermodynamic model.

3 EXPERIMENTAL SET-UP

3.1 Materials

The OPC used in this study was a CEM I 42.5 Portland cement with a Blaine fineness of 573 m^2/kg. The oxide composition of the cement determined by XRF is given in Table 1.

Chloride exposure solutions were prepared with NaCl, $CaCl_2$ and $MgCl_2$. The following three mother solutions were made: 5 M NaCl, 2.5M $CaCl_2$ and 2.5 M $MgCl_2$. The chloride content of these mother solutions was verified by titration and they were further diluted to solution with the following chloride concentrations: 0.5, 1.0, 1.5, 2.0, 2.5, 3.0 and 3.5 M.

3.2 Sample preparation

Cement paste with the CEM I 42.5 and w/c 0.4 was prepared according to [14]. It was cured spread out in sealed plastic bags in a water bath at 5°C for the first 3 days and at 20°C for the following 4 days. The resulting cement paste was crushed with a jaw crusher, and subsequently ground to 1 mm fine particles in a rotating disc mill. The resulting powder was stored in 1 l polypropylene bottles with air tight screw caps and an additional 40% water of powder mass was added to the bottles. The bottles were shaken and the paste was cured at 20°C for an additional 7 days. The moist hardened cement paste was batch-wise entered into transparent plastic bags, spread on a metal plate, and crushed by a hammer. The resulting samples, looking like “moist sand”, were homogenized and stored air tight in 1 l polypropylene bottles until analysis. This procedure aimed to maximize the degree of hydration of the cement paste and minimize carbonation.

The content of free water present in the wet paste and the degree of hydration was determined using TGA. Approx. 400 mg of the wet paste was weighed into a 900 µl alumina crucible and dried in the DTA/TG at 105°C while purging with N_2 for 4 h at which the weight of the sample had stabilized. The measured weighed loss i.e. the free water content was measured to 59% of the weight at 105°C. Immediately after, the sample was heated up at a rate of 10°C/min from 105 to 1000°C. The measured

111 weight loss in this interval, i.e. the bound water content, was 21% relative to the weight at 1000°C,
112 indicating a high degree of reaction. The hydrated cement paste had not carbonated during the processes
113 as there was no distinct increase in the weight loss peak detected with the TGA in the carbonate
114 decomposition temperature range (600-800°C).
115
116 For the determination of the chloride binding isotherms, 30 g of the hydrated cement paste (w/c = 0.96)
117 was weighed into 45 ml plastic bottle and 15 ml of the chloride containing solution was added. The
118 samples were shaken regularly and stored at 20°C for 2 months prior to analysis.
119

120 ### 3.3 Methods

121 When the samples were taken out for analysis, they were shaken and subsequently centrifuged. The
122 clear supernatant was analysed for chloride content by potentiometric titration using a Titrando 905 from
123 Metrohm; the pH of the supernatant was determined with a Metrohm 6.0255.100 Profitrode; and the
124 elemental composition Al, Ca, Cl, Fe, K, Na, Mg, S and Si was determined by ICP-MS (inductively-
125 coupled plasma mass spectrometry).
126
127 The cement pastes of the samples to which 3 M chloride solutions was added were further analysed. For
128 comparison a cement paste in contact with only distilled water was also investigated.
129
130 The moist paste was covered with Kapton© tape and analysed by XRD using a Bruker AXS D8 Focus
131 with a Lynxeye super speed detector operating at 40 kV and 40 mA. A CuKα source ($\lambda CuK\alpha = 1.54$ Å)
132 with a 0.2 mm slit was used. The scan was performed between 5 and 75° 2θ with an increment of 0.02
133 and a scanning speed of 0.5 s/step. The scans are used qualitatively to detect changes in crystalline
134 phases.
135
136 The thermogravimetric analysis (TGA) was performed with a Mettler Toledo TGA/SDTA851, on moist
137 paste samples of approximately 300 mg loaded in 900 µl alumina crucibles. The samples were dried for

2 hours at 40°C in the TGA while purging with 50ml/min N_2. After that the samples were heated from 40 to 1100°C at a rate of 10°C/min while purging with N_2.

Polished sections were prepared from paste samples which were dried for 4 days in a desiccator with silica gel prior to epoxy impregnation. They were investigated with a JEOL JSM-7001F field emission scanning electron microscope combined with a Genesis energy dispersive spectrometer (EDS) operated at an accelerating voltage of 15 kV. EDS point analysis was performed in order to investigate the phase composition. Two inherent errors to this method are: (1) the possible precipitations of ions from the pore solution on the hydrates during the drying process, causing increased concentrations of the ions; and (2) washing out of ions during the polishing process, causing decreased concentrations [15].

The changes in the phase assemblage of the binder due to contact with the exposure solutions were modelled using the Gibbs free energy minimization program, GEMS [16]. The thermodynamic data from the PSI-GEMS database [17, 18] was supplemented with cement specific data [19-23]. GEMS computes the equilibrium phases in a multi-component system based on the bulk composition of the materials. The following simplifications of the system were made in the model:

- 10% of the OPC was assumed not to have reacted.
- The C_4AF was assumed unreactive; hence no Fe containing AFm and AFt phases were predicted
- The formation of thaumasite and hydrotalcite was blocked.
- The composition of the C-S-H is a solid solution of tobermorite and jennite. S and Cl binding in the C-S-H was not taken into account.
- The soluble alkali content of the cement was adapted to fit the pH of the cement paste sample exposed to distilled water.
- Friedel's salt is assumed to be a solid solution of a calcium aluminate hydrate, monocarbonate and Friedel's salt based on the findings from [22].

4 RESULTS AND DISCUSSION

Chloride binding isotherms for the well hydrated cement pastes exposed to $MgCl_2$, $CaCl_2$ and NaCl solutions of varying chloride concentrations are given in Figure 1. In line with earlier observations [9, 10, 12] the associated cation is observed to affect the chloride binding. Mg and Ca increased the chloride binding capacity significantly compared with Na.

A selection of samples was also analyzed after 4 and 6 months. The same amount of bound chlorides was measured thereby confirming that equilibrium was reached after 2 months.

Figure 2 illustrates the measured pH of the supernatants, and in Figure 3 a direct relationship between the pH of the supernatant and the amount of bound chloride can be observed. It should be noted that the impact of the pH on chloride binding has been observed by others [5, 9, 24]. However the direct relationship depicted in Figure 3 showing a decreased binding for increased pH independently of the associated cation illustrates undoubtfully the dominating effect of pH on chloride binding.

Figure 4, Figure 5 and Figure 6 show the volume of the different hydration phases predicted by the thermodynamic model GEMS as function of the Cl concentration of the exposure solutions with respectively $CaCl_2$, $MgCl_2$ and NaCl. The changes in the AFm and AFt phases as function of the Cl concentration of the exposure solution are quite similar for the different associate cations. The AFm and AFt phases predicted to form in the sample exposed to only distilled water (chloride concentration 0 mol/l) are monosulphate, hemicarbonate and ettringite. When the Cl concentration increases, monosulphate decomposes to form Kuzel's salt and ettringite. At concentrations going from approx. 0.01 mol/l, the hemicarbonate and Kuzel's salt are replaced with Friedel's salt and the sulphates formerly bound in monosulphate and Kuzel's salt are bound in ettringite.

Figure 7 shows the variations in the amount of $Ca(OH)_2$ and $Mg(OH)_2$ formed as function of the concentration of the added solutions. Upon addition of the $MgCl_2$ solution, the $MgCl_2$ reacts with an equimolar amount of $Ca(OH)_2$ and $Mg(OH)_2$ precipitates. In the case of $CaCl_2$ addition the amount of

192 $Ca(OH)_2$ in the system increases slightly whereas in the case of NaCl addition the amount of $Ca(OH)_2$
193 decreases slightly
194
195 Figure 8 shows the predicted Ca and S concentration in the exposure solutions, and Figure 16 is showing
196 the modelled and measured pH of the corresponding systems. The changes in the pH and the
197 concentration of the Ca and S are closely interrelated. In the case of exposure to $MgCl_2$ and $CaCl_2$
198 solutions, the pH was dropping from approx. 13.2 to 12.2 with increasing concentration of the added
199 solutions. For the NaCl solutions first an increase of the pH was observed to almost 13.4 followed by a
200 slight decrease from Cl concentrations higher than 1 mol/l to approx. 13.3. The lowering of the pH in
201 the $CaCl_2$ and $MgCl_2$ systems results in a higher solubility of Ca (see Figure 8). The $Ca(OH)_2$
202 precipitated in the $CaCl_2$ and $MgCl_2$ system will therefore dissolves partially. Hence the amount of
203 additionally formed $Ca(OH)_2$ or $Ca(OH)_2$+$Mg(OH)_2$ is not equimolar to the amount of $CaCl_2$ or $MgCl_2$
204 added to the system as earlier suggested by Tritthart in [9] (see Figure 7). The concentration of S in the
205 exposure solution is expected to increase with increasing Cl concentration as Cl-AFm phases are
206 thermodynamically favoured compared to S-AFm [22]. Hence S is being released from the AFm phases
207 and its concentration in the exposure solution increases. The difference in S concentration between the
208 NaCl and the $CaCl_2$ or $MgCl_2$ systems (see Figure 15) is due to the pH differences. The lower pH in the
209 latter two systems stabilizes ettringite, thereby more ettringite is formed and the S concentration
210 lowered.
211
212 The solid phases in the cement paste to which 3 M chloride solutions were added were analyzed and
213 compared to the solid phases of cement paste exposed to water only. The TG curves from the cement
214 paste exposed to $MgCl_2$ (Figure 9) show the formation of $Mg(OH)_2$ and consumption of $Ca(OH)_2$ as
215 expected. Changes in the AFm phases upon exposure to the chloride solutions are observed from TG
216 curves, XRD spectra and SEM-EDS dot plots. The XRD spectra (Figure 10) indicate the formation of
217 Cl-AFm, and the SEM-EDS plot (Figure 12) confirms this. Concerning the AFt phases, the XRD spectra
218 (Figure 10) indicate their presence, whereas AFt cannot be observed in the SEM-EDS plot (Figure 13).
219 In addition to changes in the AFm phases also changes in the composition of the C-S-H can be observed

220 in the SEM-EDS plots. The chloride binding in the C-S-H appears to depend on the associated cation;
221 an increased chloride content is observed in the C-S-H of the cement pastes exposed to Mg and Ca
222 (Figure 11). Also, changes appear to take place in the Si/Ca and the S/Ca ratios, which are lower and
223 higher, respectively, in the cement pastes exposed to Mg and Ca compared to the Na and water exposed
224 pastes (Figure 12 and Figure 13).
225
226 **Comparison of measured and modelled compositions**
227 The solid phase composition predicted by GEMS, for the cement paste in contact with the exposure
228 solutions tested consists of a constant amount of C-S-H, a varying amount of CH and varying types and
229 amounts of AFm and AFt phases (see Figure 4 to Figure 6).
230
231 The AFm phases predicted by GEMS in the system of the cement paste with distilled water are
232 monosulphate and hemicarbonate. This is in agreement with the SEM-EDS graph (Figure 13) and the
233 double peak in the XRD spectrum (see Figure 10). Upon increasing Cl concentration changes take place
234 in the AFm and AFt phases. Monosulphate and hemicarbonate transform partly to Friedel's salt (see
235 equation 1 and 3[1]) where Kuzel's salt can be an intermediate state. Part of the released sulphates are
236 bound in ettringite (equation 2) and part of the released carbonates are bound in monocarbonate
237 (equation 4).
238
239 The AFm and AFt phases predicted to form when for the cement paste to which 3 M chloride solution
240 was added are ettringite combined with monocarbonate and Friedel salt. The presence of ettringite and
241 a Cl-AFm phase was confirmed by XRD (see Figure 10). The SEM-EDS results indicated that the Cl-
242 AFm is a mixture of Friedel's salt and a carbonate AFm, as predicted by the model.
243
244 $C_4A\underline{S}H_{12} + 2\ Cl^- \rightarrow C_4ACl_2H_{10} + \underline{S}^{2-}$ (1)

[1] Notation for equations 1-5: C=CaO, A=Al_2O_3, $\underline{S}$=SO_3^{2-}, H=H_2O, Cl=Cl^-, $\underline{C}$=CO_2^{2-}

$$C_4A\underline{S}H_{12} + 2\ \underline{S}^{2-} + 2\ CH + 20\ H \rightarrow C_6A\underline{S}_3H_{32} + 4\ OH^- \quad (2)$$

$$C_4A\underline{C}_{0.5}H_{12} + 2\ Cl^- \rightarrow C_4ACl_2H_{10} + 0.5\ \underline{C}^{2-} + OH^- \quad (3)$$

The following mechanisms explaining the changes in the pH for the NaCl, $MgCl_2$ and $CaCl_2$ exposure solutions, affecting the binding capacity of the tested cement paste, are suggested:

For $CaCl_2$ exposure solutions an acidification of the system and the formation of $Ca(OH)_2$ is observed. The proposed simplified reaction is described with equation (4). The $Ca(OH)_2$ will precipitate as the system is already saturated with it. However, the pH reduction of the system will result in a higher solubility of Ca. Hence, the precipitation of $Ca(OH)_2$ is not equimolar with the amount of $CaCl_2$ added as has been stated earlier [9].

$$CaCl_2 + 2\ OH^- \rightarrow Ca(OH)_2 \downarrow + 2\ Cl^- \quad (4)$$

In the case where a $MgCl_2$ solution is used as exposure solution, the $MgCl_2$ will react with $Ca(OH)_2$ and will precipitate equimolarly as brucite $Mg(OH)_2$ (see equation 4 and Figure 7). The $CaCl_2$ formed will react further according to equation 4. Hence the changes in the pH in the $MgCl_2$ system are similar to the $CaCl_2$ system.

$$MgCl_2 + Ca(OH)_2 \rightarrow Mg(OH)_2 \downarrow + CaCl_2 \quad (5)$$

For exposure solutions with NaCl, it has been claimed [13, 25] that the NaCl will react with the $Ca(OH)_2$, which is in excess in the system and form NaOH and $CaCl_2$. The $CaCl_2$ formed should then react with e.g. C_3A and form Friedel's salt or Kuzel's salt, and the NaOH would result in a higher pH of the exposure solution. However, there is no pH increase associated with the formation of Friedel's salt from monosulphate or monocarbonate. This involves only an ions exchange between SO_4^{2-} or CO_3^{2-} with 2

Cl^- and not the production of hydroxide. The pH increase observed in the NaCl system is caused by changes in the AFm and AFt phases such as the formation of ettringite from monosulphate (see equation 2) or Friedel's salt from hemicarbonate (see equation 3) which supplies additional OH^- to the system. Hence, there would be no pH increase for NaCl exposure solutions if the system was over-sulphated even though Friedel's salt would form. According to equation (2), the transformation of monosulphate to ettringite consumes $Ca(OH)_2$. This is in line with the observed decrease in $Ca(OH)_2$ for the NaCl system in Figure 7.

Figure 16 and Figure 15 show that the trends observed in the measured and modelled composition of the exposure solutions at equilibrium agree fairly well for the samples with 3 M Cl added solutions and distilled water. The composition of the exposure solutions are reflected in the Na, Cl and Ca content, except that also the supernatant from the $MgCl_2$ exposed sample has increased Ca content. An increase in the S content can be observed for the supernatant with NaCl.

The underestimation of the decrease of the predicted pH compared to the measured pH for $MgCl_2$ and $CaCl_2$ at added concentrations higher than 2 mol/l (see Figure 16) might be due to changes in the C-S-H composition which are not taken into account in the model. The SEM-EDS measurements indicate an increase in the Ca/Si ratio of the C-S-H for $MgCl_2$ and $CaCl_2$ solutions (see Figure 12). This might lead to an increase in the adsorption of OH^- ions on the C-S-H and hence a lowering of the pH.

From Figure 17 it can be seen that there is a significant difference between the modelled and measured amount of bound chlorides. It should be noted that the amount of aluminate phases which bind chlorides seems to be overestimated. However, the main difference between the modelled and measured amount of bound chlorides can be attributed to the binding of chlorides by the C-S-H which is not taken into account in the model. It can be concluded that the binding of Cl in the C-S-H contributes considerably to the total amount of chlorides bound by cement paste, and that the Cl binding in the C-S-H is strongly dependent on the pH of the exposure solution (see Figure 3). There is a need for a refined thermodynamic

300 model for Cl binding in the C-S-H phase and further experimental data to further understand the
301 mechanisms of Cl binding in the C-S-H.
302
303 The practical relevance of these findings lays in the application of data for chloride binding. Ponding
304 experiments with NaCl solution or sea water show that Na enters the concrete only in the first 50 µm
305 whereas chlorides can penetrate several cm [26]. Hence, binding of chloride inside the concrete takes
306 place in the absence of Na. In order to maintain the charge balance an ion exchange between Cl^- and
307 OH^- takes place upon chloride ingress, leading to variations in the pH from the exposed concrete surface.
308 Hence, binding isotherms measured with NaCl solutions [2-7] will result in a conservative estimate of
309 the amount of bound chlorides.

5 CONCLUSION

The chloride binding isotherms determined for the well hydrated cement pastes exposed to $MgCl_2$, $CaCl_2$ and NaCl solutions confirmed that the associated cation strongly affects the chloride binding. In-line with literature Mg^{2+} and Ca^{2+} increased the chloride binding capacity significantly compared to Na^{+}.

A linear relation between the pH of the exposure solution and the chloride binding was observed. The relationship is independent of the cation. Therefore the key to understanding the impact of the associate cation on chloride binding lays in the changes in the pH of the exposure solution.

The thermodynamic model predicted that when the cement paste is exposed to $CaCl_2$ or $MgCl_2$, respectively $Ca(OH)_2$ or $Mg(OH)_2$ will precipitate, leading to a reduction in pH and a consequent increase in the solubility of Ca. The predictions were confirmed by pH measurements and elemental analysis (ICP-MS) of the exposure solution. The SEM-EDS analysis showed that the lower pH and higher Ca concentration of the exposure solution leads to a higher C/S ratio and a higher chloride content of the C-S-H phase.

In the case of the NaCl exposure solutions the pH and the C-S-H composition did not change considerably compared to the sample exposed to distilled water. However, a slight increase in pH was observed at low chloride concentrations. The thermodynamic model indicated that this could be caused by changes in the AFm and AFt phases.

The thermodynamic model predicted that binding of chlorides in chloroaluminate hydrates such as Friedel's and Kuzel's salts is not greatly affected by the cation associated with the chloride.

It can be concluded that C-S-H plays a major role regarding chloride binding in cement paste, and that the chloride binding capacity of the C-S-H is strongly depended on its composition, which is affected by the exposure solution and thereby

6 ACKNOWLEDGEMENTS

The authors would like to acknowledge COIN, the COncrete INnovation center (www.coinweb.no), for facilitating this research project. Julian Tolchard is gratefully acknowledged for facilitating and assisting with the scanning electron microscope investigations. Syverin Lierhagen from NTNU Faculty of Science and Technology Department Chemistry is acknowledged for performing the ICP-MS analyses on the dissolved concrete samples. Special thanks go to Barbara Lothenbach for the training and support received when working with GEMS.

7 REFERENCES

[1] C.M. Hansson, T. Frølund, J.B. Markussen, The effect of chloride cation type on the corposion of steel in concrete by chloride salts, Cement Concrete Res, 15 (1985) 65-73.

[2] C.L. Page, P. Lambert, P.R.W. Vassie, Investigations of reinforcement corrosion. 1. The pore electrolyte phase in chloride-contaminated concrete, Mater Struct, 24 (1991) 243-252.

[3] C. Larsen, Chloride binding in concrete. Effect of surrounding environment and concrete composition, in, PhD Thesis, Norwegian University of Science and Technology, Trondheim, 1998.

[4] O.M. Jensen, M.S.H. Korzen, H.J. KJakobsen, J. Skibsted, Influence of cement constitution and temperature on chloride binding in cement paste, Advances in cement research, 12 (2000) 57-64.

[5] H. Zibara, Binding of external chlorides by cement paste, in: Department of Civil Engineering, University of Toronto, National Library of Canada, 2001.

[6] H. Zibara, R.D. Hooton, M.D.A. Thomas, K. Stanish, Influence of the C/S and C/A ratios of hydration products on the chloride ion binding capacity of lime-SF and lime-MK mixtures, Cement Concrete Res, 38 (2008) 422-426.

[7] M.D.A. Thomas, R.D. Hooton, A. Scott, H. Zibara, The effect of supplementary cementitious materials on chloride binding in hardened cement paste, Cement Concrete Res, 42 (2012) 1-7.

[8] Statensvegvesen, Salt Smart - Miljøkonsekvenser ved salting av veger - en litteraturgjennomgang in: Teknologirapport 2535 Geoteknikk-og skredsekjsonen, www.statensvegvesen.no, 2008, pp. 98.

[9] J. Tritthart, Chloride binding in cement II. The influence of the hydroxide concentration in the pore solution of hardened cement paste on chloride binding, Cement Concrete Res, 19 (1989) 683-691.

[10] C. Arya, N.R. Buenfeld, J.B. Newman, Factors influencing chloride-binding in concrete, Cement Concrete Res, 20 (1990) 291-300.

[11] A. Delagrave, J. Marchand, J.-P. Ollivier, S. Julien, K. Hazrati, Chloride binding capacity of various hydrated cement paste systems, Advanced Cement Based Materials, 6 (1997) 28-35.

[12] O. Wowra, M.J. Setzer, Sorption of chlorides on hydrates cement and C_3S pastes, in: M.J. Setzer, R. Auberg (Eds.) Frost resistance of concrete, E & FN Spon, London, 1997, pp. 147-153.

371 [13] Q. Zhu, L. Jiang, Y. Chen, J. Xu, L. Mo, Effect of chloride salt type on chloride binding behavior
372 of concrete, Construction and Building Materials, 37 (2012) 512-517.
373 [14] H. Justnes, M.R. Geiker, A critical view on serice life predictions based on chloride induced
374 corrosion, in: 2nd International Conference on Micro Durability "Microstructure related durability
375 of cementitious composites", Amsterdam 2012.
376 [15] K. De Weerdt, M.R. Geiker, H. Justnes, 10 year old concrete wall in tidal zone examined by SEM-
377 EDS - submitted, in: U. Hjorth Jakobsen (Ed.) 14th Euroseminar on microscopy applied ot building
378 materials, Helsingør, Denmark, 2013.
379 [16] D. Kulik, GEMS 2 software, http://gems.web.psi.ch/, in, PSI, Villingen, Switzerland, 2010.
380 [17] T. Thoenen, D. Kulik, Nagra/PSI chemical thermodynamic database 01/01 for GEMS-selektor
381 (V.2-PSI) geochemical modeling code, http://gems.web.psi.ch/doc/pdf/TM-44-03-04-web.pdf, in,
382 PSI, Villingen, 2003.
383 [18] W. Hummel, U. Berner, E. Curti, F.J. Pearson, T. Thoenen, Nagra/PSI chemical thermodynamic
384 data base 01/01, in, Universal Publishers/uPUBLISH.com, USA also published as Nagra Tehcnical
385 Report NTB 02-16, Wettingen, Switzerland, 2002.
386 [19] B. Lothenbach, F. Winnefeld, Thermodynamic modelling of the hydration of Portland cement,
387 Cement Concrete Res, 36 (2006) 209-226.
388 [20] T. Matschei, B. Lothenbach, F.P. Glasser, Thermodynamic properties of Portland cement hydrates
389 in the system $CaO-Al_2O_3-SiO_2-CaSO_4-CaCO_3-H_2O$, Cement Concrete Res, 37 (2007) 1379-1410.
390 [21] B. Lothenbach, T. Matschei, G. Möschner, F.P. Glasser, Thermodynamic modelling of the effect
391 of temperature on the hydration and porosity of Portland cement, Cement Concrete Res, 38 (2008)
392 1-18.
393 [22] M. Balonis, B. Lothenbach, G. Le Saout, F.P. Glasser, Impact of chloride on the mineralogy of
394 hydrated Portland cement systems, Cement Concrete Res, 40 (2010) 1009-1022.
395 [23] B.Z. Dilnesa, B. Lothenbach, G. Le Saout, G. Renaudin, A. Mesbah, Y. Filinchuk, A. Wichser, E.
396 Wieland, Iron in carbonate containing AFm phases, Cement Concrete Res, 41 (2011) 311-323.
397 [24] P. Henocq, E. Samson, J. Marchand, Portlandite content and ionic transport properties of hydrated
398 C3S pastes, Cement Concrete Res, 42 (2012) 321-326.

[25] M. Ben-Yair, The effect of chlorides on concrete in hot and arid regions, Cement Concrete Res, 4 (1974) 405-416.

[26] K. De Weerdt, D. Orsakova, M.R. Geiker, Comparing chloride ingress in concrete exposed to sea water and NaCl solution testing different cement types, in: COIN reports, NTNU/SINTEF, www.coinweb.no, 2013.

406 Tables

407 Table 1 - Oxide composition of the CEM I 42.5 used in the experiments.

Composition	[%]
SiO_2	19.8
Al_2O_3	5.2
Fe_2O_3	3.5
CaO	61.5
MgO	2.7
SO_3	3.6
K_2O	1.2
Na_2O	0.5
total Cl	0.056
CO_2	0.35
LOI	1.11
Free Lime	1.4

408

409

410

411

412 Figures

413 Figure 1: Chloride binding isotherms for pastes exposed to $MgCl_2$, $CaCl_2$ and NaCl at 20°C.

414 Figure 2: pH as function of the chloride concentration in the exposure solution for pastes exposed to
415 $MgCl_2$, $CaCl_2$ and NaCl at 20°C

416 Figure 3: Bound chloride vs. pH in pastes exposed to $MgCl_2$, $CaCl_2$ and NaCl.

417 Figure 4 : Modelled volume of hydration phases as function of concentration of added $CaCl_2$ solution.

418 Figure 5 : Modelled volume of hydration phases as function of concentration of the added $MgCl_2$
419 solution

420 Figure 6 : Modelled volume of hydration phases as function of concentration of added NaCl solution.

421 Figure 7 : Modelled amount of $Ca(OH)_2$ and $Mg(OH)_2$ as function of the Cl concentration of the added
422 solution.

423 Figure 8 : Modelled concentration of Ca and S in the exposure solution as function of the Cl
424 concentration in the added solution

425 Figure 9 - TG and DTG curves of the cement pastes exposed to water and the 3M chloride exposure
426 solutions

427 Figure 10 - XRD spectra in the range 5-20 2theta of the cement pastes exposed to water and the 3M
428 chloride exposure solutions

429 Figure 11 - SEM-EDS results showing the Cl/Ca as function of the Al/Ca ratio.

430 Figure 12 - SEM-EDS results showing the Al/Ca ratio as function of the Si/Ca ratio

431 Figure 13 - SEM-EDS results showing the S/Ca ratio as function of the Al/Ca ratio.

432 Figure 14 - Measured concentration of Na, Cl, Ca and S in the exposure solution.

433 Figure 15 – Comparing modeled and measured concentration of Na, Cl, Ca and S in the exposure
434 solution.

435 Figure 16 - Comparison between measured and modelled pH as function of the Cl concentration in the
436 added solution.

437 Figure 17 - Comparison between measured and modelled amount of bound chlorides as function of the
438 Cl concentration in the added solution.

439

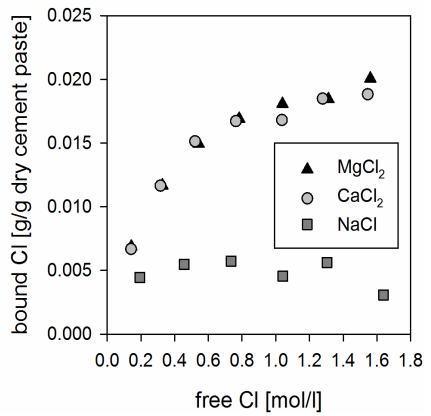

440

441 Figure 1: Chloride binding isotherms for pastes exposed to $MgCl_2$, $CaCl_2$ and NaCl at

442 20°C.

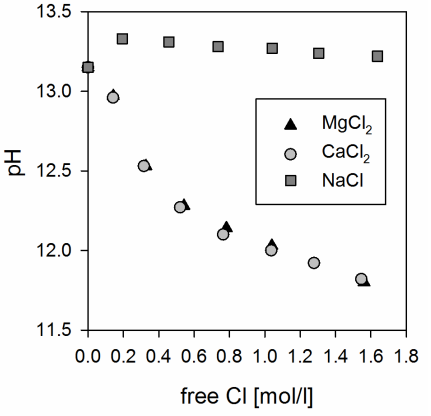

443

444 Figure 2: pH as function of the chloride concentration in the exposure solution for pastes exposed to

445 $MgCl_2$, $CaCl_2$ and NaCl at 20°C

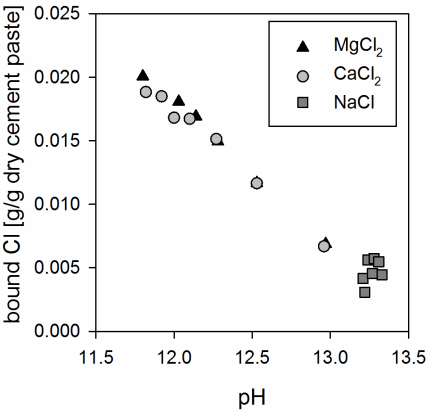

446

447 Figure 3: Bound chloride vs. pH in pastes exposed to $MgCl_2$, $CaCl_2$ and NaCl.

448

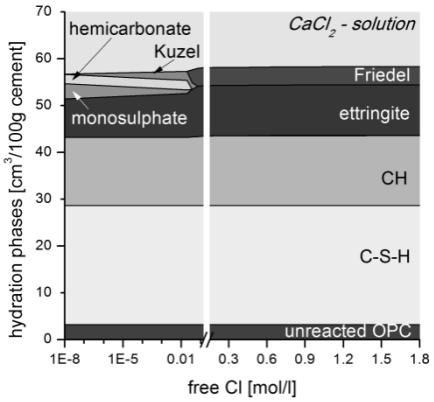

Figure 4 : Modelled volume of hydration phases as function of concentration of added $CaCl_2$ solution.

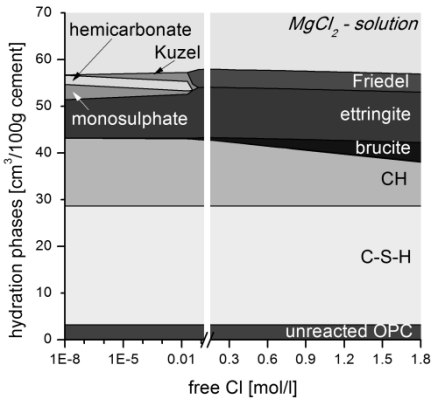

Figure 5 : Modelled volume of hydration phases as function of concentration of the added $MgCl_2$ solution

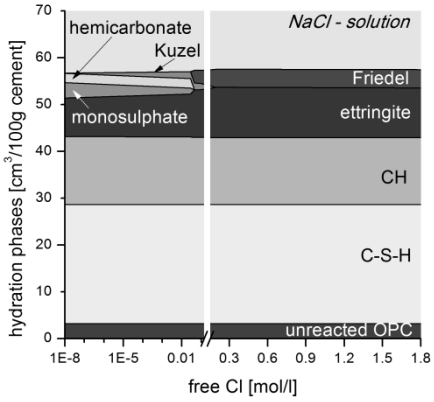

Figure 6 : Modelled volume of hydration phases as function of concentration of added NaCl solution.

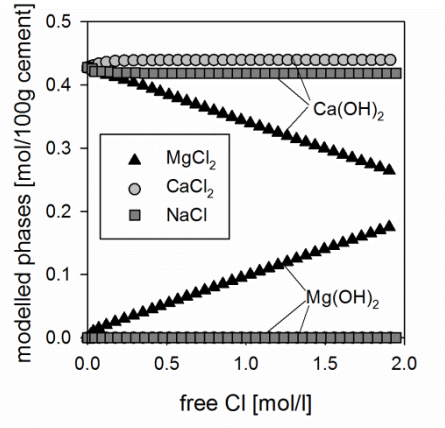

Figure 7 : Modelled amount of $Ca(OH)_2$ and $Mg(OH)_2$ as function of the Cl concentration of the added solution.

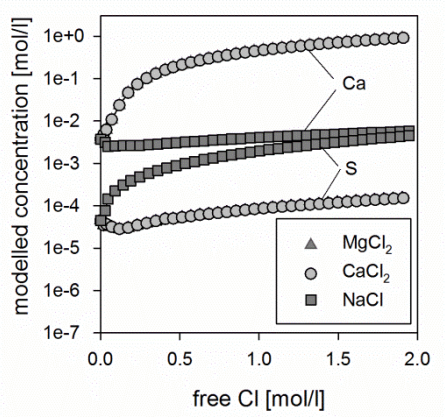

Figure 8 : Modelled concentration of Ca and S in the exposure solution as function of the Cl concentration in the added solution

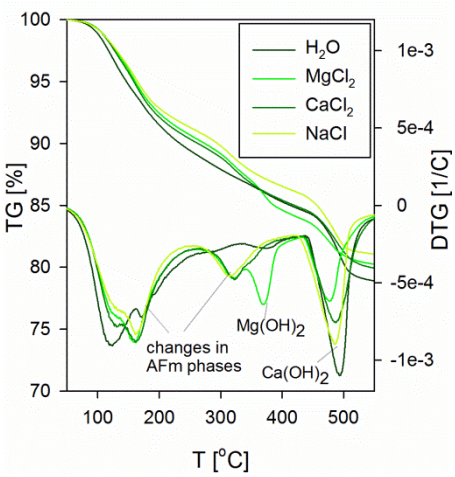

Figure 9 - TG and DTG curves of the cement pastes exposed to water and the 3M chloride exposure solutions

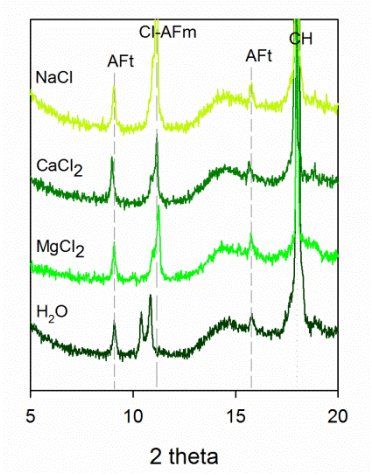

Figure 10 - XRD spectra in the range 5-20 2theta of the cement pastes exposed to water and the 3M chloride exposure solutions

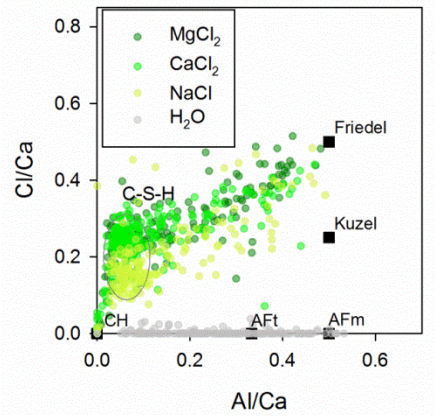

Figure 11 - SEM-EDS results showing the Cl/Ca as function of the Al/Ca ratio.

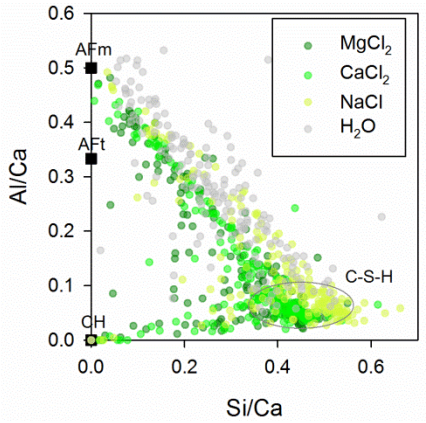

Figure 12 - SEM-EDS results showing the Al/Ca ratio as function of the Si/Ca ratio

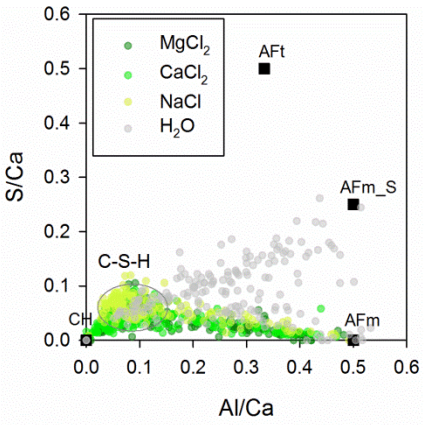

Figure 13 - SEM-EDS results showing the S/Ca ratio as function of the Al/Ca ratio.

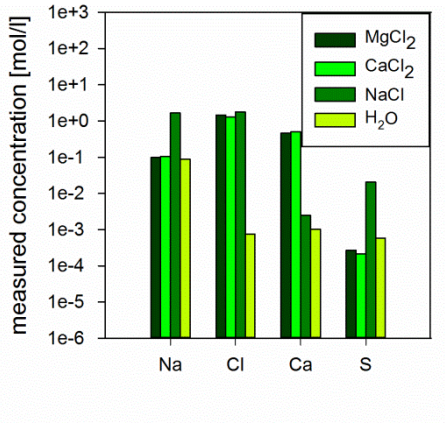

Figure 14 - Measured concentration of Na, Cl, Ca and S in the exposure solution.

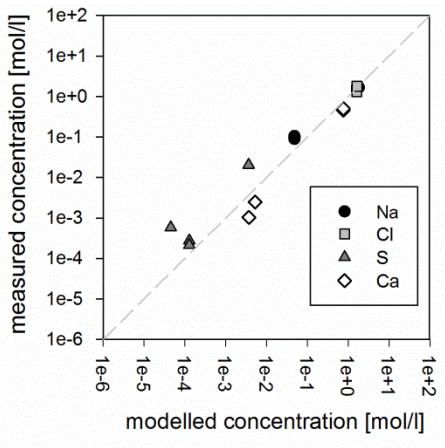

Figure 15 – Comparing modeled and measured concentration of Na, Cl, Ca and S in the exposure solution.

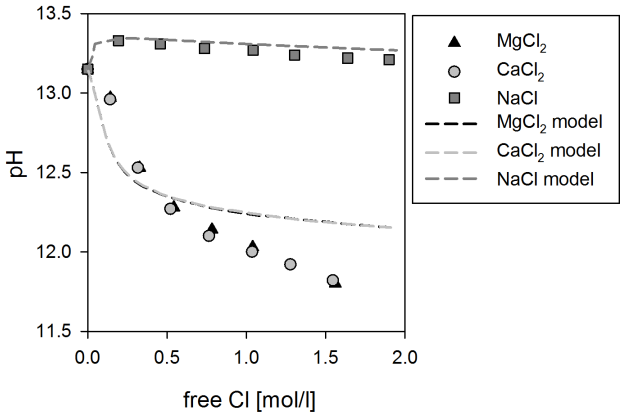

Figure 16 - Comparison between measured and modelled pH as function of the Cl concentration in the added solution.

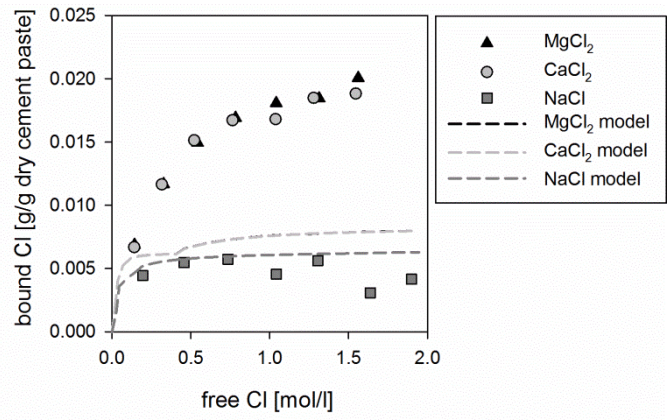

Figure 17 - Comparison between measured and modelled amount of bound chlorides as function of the Cl concentration in the added solution.